Comparison of Hydrodynamic Load Predictions Between Engineering Models and Computational Fluid Dynamics for the OC4-DeepCwind Semi-Submersible

Preprint

Maija A. Benitz, David P. Schmidt, Matthew A. Lackner, and Gordon M. Stewart
University of Massachusetts

Jason Jonkman and Amy Robertson
National Renewable Energy Laboratory

Presented at the ASME 2014 33rd International Conference on Ocean, Offshore and Arctic Engineering (OMAE2014)
San Francisco, California
June 8–13, 2014

NREL is a national laboratory of the U.S. Department of Energy
Office of Energy Efficiency & Renewable Energy
Operated by the Alliance for Sustainable Energy, LLC

This report is available at no cost from the National Renewable Energy Laboratory (NREL) at www.nrel.gov/publications.

Conference Paper
NREL/CP-5000-61157
September 2014

Contract No. DE-AC36-08GO28308

NOTICE

This report is available at no cost from the National Renewable Energy Laboratory (NREL) at www.nrel.gov/publications.

Available electronically at http://www.osti.gov/scitech

Available for a processing fee to U.S. Department of Energy and its contractors, in paper, from:

U.S. Department of Energy
Office of Scientific and Technical Information
P.O. Box 62
Oak Ridge, TN 37831-0062
phone: 865.576.8401
fax: 865.576.5728
email: mailto:reports@adonis.osti.gov

Available for sale to the public, in paper, from:

U.S. Department of Commerce
National Technical Information Service
5285 Port Royal Road
Springfield, VA 22161
phone: 800.553.6847
fax: 703.605.6900
email: orders@ntis.fedworld.gov
online ordering: http://www.ntis.gov/help/ordermethods.aspx

Cover Photos: (left to right) photo by Pat Corkery, NREL 16416, photo from SunEdison, NREL 17423, photo by Pat Corkery, NREL 16560, photo by Dennis Schroeder, NREL 17613, photo by Dean Armstrong, NREL 17436, photo by Pat Corkery, NREL 17721.

Proceedings of the ASME 2014 33rd International Conference on Ocean, Offshore and Arctic Engineering
OMAE2014
June 8-13, 2014, San Francisco, California, USA

OMAE2014-23985

COMPARISON OF HYDRODYNAMIC LOAD PREDICTIONS BETWEEN ENGINEERING MODELS AND COMPUTATIONAL FLUID DYNAMICS FOR THE OC4-DEEPCWIND SEMI-SUBMERSIBLE

Maija A. Benitz
David P. Schmidt
Matthew A. Lackner
Gordon M. Stewart
Department of Mechanical and Industrial Engineering
160 Governor's Drive
University of Massachusetts
Amherst, Massachusetts USA 01003
(413) 545-4267
Email: mbenitz@engin.umass.edu

Jason Jonkman
Amy Robertson
National Renewable Energy Laboratory
15013 Denver West Pkwy
Golden, Colorado USA 80401

ABSTRACT

Hydrodynamic loads on the platforms of floating offshore wind turbines are often predicted with computer-aided engineering tools that employ Morison's equation and/or potential-flow theory. This work compares results from one such tool, FAST, the National Renewable Energy Laboratory's wind turbine computer-aided engineering tool, and the high-fidelity computational fluid dynamics (CFD) package, OpenFOAM, for the OC4-DeepCwind semi-submersible analyzed in the International Energy Agency Wind Task 30 project. Load predictions from HydroDyn, the offshore hydrodynamics module of FAST, are compared with results from OpenFOAM. HydroDyn uses a combination of Morison's equation and potential-flow theory to predict the hydrodynamic forces on the structure, at a small computational cost compared to CFD. The implications of the assumptions in HydroDyn are evaluated based on this code-to-code comparison.

1 INTRODUCTION

There is great potential for the growth of wind energy in offshore locations where the structures are exposed to a variety of loading from waves, current and wind [1, 2]. A variety of computer-aided engineering (CAE) tools, based largely on engineering models employing potential-flow theory and/or Morison's equation, are currently being used to evaluate hydrodynamic loading on floating offshore wind turbine platforms [3, 4]. Evaluation of the validity of these tools is a necessary step toward proper modeling. In this work, the open-source computational fluid dynamics (CFD) package, OpenFOAM, is used to provide high-fidelity simulations of wind turbine platforms in steady current and waves to assess the validity of potential-flow and Morison solutions. The volume-of-fluid (VOF) approach in CFD simulates the flow of two immiscible fluids, by advecting a fluid volume fraction and tracking the location of the fluid interface. Forces and moments on the structure are evaluated by integrating pressure and viscous stresses along the surface of the body.

FAST [5], which employs engineering models, is the National Renewable Energy Laboratory's (NREL) wind turbine CAE tool. In this paper, hydrodynamic load predictions from FAST's hydrodynamics module, HydroDyn, are compared with results from OpenFOAM for a fixed semi-submersible platform. Future work will examine loading predictions when the body is subject to full 6 degree-of-freedom motion, including radi-

ation added mass and damping. The OC4-DeepCwind semi-submersible analyzed in the International Energy Agency (IEA) Wind Task 30 project is used for this study [6]. The effects of the wind turbine are neglected.

HydroDyn uses a combination of Morison's equation with potential-flow theory to predict loads on offshore structures, including floating platforms. Morison's equation is more valid for small members where viscous and inertial effects dominate. Potential-flow theory is more appropriate for larger members where radiation and diffraction effects are more important. The interaction between the individual components of the structure is neglected. This means that the loads on the individual components are summed, but the large components do not influence the hydrodynamic loads on the small components and vice-versa. In CFD simulations the forces and moments are predicted entirely by the flow field such that interaction effects are intrinsically accounted for, but with large computational expense.

To study the implications of the assumptions in HydroDyn, both FAST and OpenFOAM were used to simulate a series of cases using a variety of wave and current conditions. Simulations of the semi-submersible are performed in each tool, and load predictions are compared. To specifically address the issue of body-size classification as well as component interaction, three meshes are used in the CFD study of the semi-submersible. The first mesh contains the entire semi-submersible geometry. The second and third meshes contain only the small and only the large members, respectively. The assumptions in HydroDyn are assessed based on the comparison of load predictions against results from OpenFOAM. Even though HydroDyn is used in this study, the results are likely applicable to other engineering codes that employ similar models.

2 ANALYSIS SPECIFICATIONS

The OC4-DeepCwind semi-submersible platform geometry is selected in this study because it is composed of both small and large components relative to the waves encountered in the ocean environment, meaning that viscous drag, static pressure, dynamic pressure, and inertial loads all contribute to the loading on the structure. (Radiation added mass and damping are neglected in this study of a stationary platform.) The specifications of the semi-submersible geometry are outlined here, followed by a description of the simulated environmental conditions. Simulations performed in OpenFOAM are conducted at 1/50th the scale of the prototype semi-submersible, such that the dimensions of the CFD mesh match the dimensions of the semi-submersible employed in the the DeepCwind tank testing campaign. The FAST simulations are carried out with full prototype scale length dimensions, but are effectively treated at model scale because of the chosen drag coefficients. To properly compare the HydroDyn results with those from OpenFOAM, the drag coefficient used in FAST is derived from the model-scale Reynolds number, and the drag coefficient is chosen to be 1.0. All dimensions, forces, and other data from OpenFOAM are presented at prototype scale, scaled using Froude scaling relationships. The Froude number is given by $Fr = \frac{u^2}{gL}$, where u is the fluid velocity, g is gravity, and L is the characteristic structure length. The scaling relationship between model and prototype is upheld by $Fr_{model} = Fr_{prototype}$. Although the Froude scaling method cannot be applied in conjunction with Reynolds number scaling, it does properly scale inertial effects [7]. This inconsistency was avoided by using a model-scale Reynolds number for the FAST simulations.

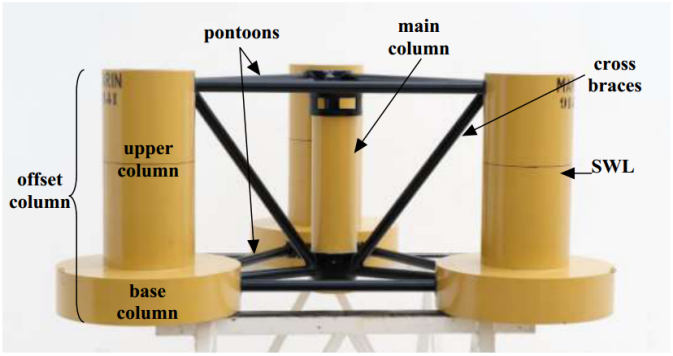

FIGURE 1. The model-scale semi-submersible, built at 1/50th the size of the prototype, from the DeepCwind tank tests with component definitions labeled [6]. Note: SWL is the still water line

2.1 Semi-Submersible Specifications

Discussions of the tower or turbine properties are neglected because these simulations omit the wind turbine. The semi-submersible structure, built at model scale and used in the DeepCwind tank tests, is shown in Fig. 1 with labeled components. The three large cylinders are referred to as the offset columns, and are split into the upper and base columns. The center of the semi-submersible consists of a single main column that is connected to the offset columns with pontoons and cross braces. Additionally, the still water line (SWL) is indicated on the right offset column. The dimensions of the individual components, at prototype scale, are given in Table 1.

2.2 Representative Geometries

HydroDyn predicts wave and current loads on offshore structures using Morison's equation in conjunction with potential-flow theory. For small members, where it is assumed that viscous and inertial forces dominate, Morison's equation is most appropriate. For the larger members, where diffraction effects become dominant, potential-flow theory is more valid (based on a preprocess using a panel method such as WAMIT). To study the implications of the applicability of Morison's equa-

TABLE 1. Specifications of the semi-submersible structure [6]

Depth of platform base below SWL (total draft)	20.0 m
Centerline spacing between offset columns	50.0 m
Length of upper columns	26.0 m
Length of base columns	6.0 m
Diameter of main column	6.5 m
Diameter of offset (upper) columns	12.0 m
Diameter of base columns	24.0 m
Diameter of pontoons and cross braces	1.6 m

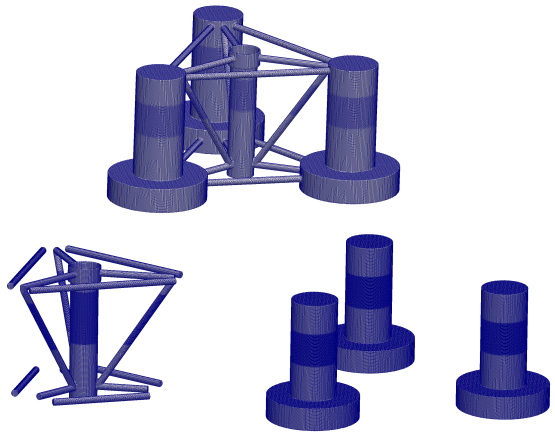

FIGURE 2. The surfaces of the semi-submersible from the full geometry, large components only and small components only numerical meshes for CFD, in clockwise order from the top

tion and potential-flow theory as they relate to the component size, CFD simulations are performed on three representative geometries that include all components, only the small components and only the large components. High-fidelity results from the three CFD meshes are compared against results from HydroDyn where distinction between body size alters the limits of applicability for the CAE model equations. In OpenFOAM, the validity of the model equations does not change based on structure size, so the representative geometry is changed instead.

First, a mesh representing the entire semi-submersible platform is generated. The surface of the semi-submersible is shown in the top of Figure 2, where an increased level of refinement can be seen around the SWL. This mesh is referred to as the "Full Geometry" throughout this study. Next, the offset columns are isolated from the pontoons, cross braces, and main column, to generate the geometry shown in the bottom right of Fig. 2, where again, a region of increased mesh refinement exists around the SWL. This mesh is referred to as "large components only." Finally, the cross braces, pontoons, and main column compose the "small components only" mesh, which is shown at the bottom left of Fig. 2. The following sections give more detail on categorizing the individual components as small or large.

2.3 Environmental Conditions

The semi-submersible is simulated in a variety of environmental conditions to examine a range of loading regimes. First, a series of current-only cases are carried out. The current velocity ranges from 0.3 m/s to 1 m/s at prototype scale, and these velocities are scaled down to model scale with Froude scaling. This range of current velocities is selected because it matches the conditions most likely to be found in the ocean environment. The values for the current velocities are given in Table 2, at both model and prototype scale. Additionally, the Reynolds numbers for each of the four major components of the semi-submersible are given at each of the current velocities.

Confidence in the ability to predict loads on bodies in steady flow, such as current, is high. A more detailed discussion of validation cases is given in Section 3.2.4, where Fig. 4 demonstrates the ability to predict the drag coefficient of a vertical cylinder over a range of Reynolds numbers. For added clarity, the ranges of Reynolds numbers at model and prototype scale are indicated in Fig. 4.

In addition to simulating the semi-submersible in a range of current conditions, a variety of wave conditions are investigated. The properties for three simulated wave cases are shown in Table 3. The simulated wave cases span a wave height range from 1.95 m to 2.75 m, and a range of periods from 7.5 s to 8.8 s, at prototype scale. The wave simulations carried out in this work fall between sea states 3 and 5.

2.4 Categorization of Component Size

The four major components of the semi-submersible can be mapped onto a plot of the Keulegan-Carpenter number versus the diffraction parameter, which depend on both the wave parameters and structure size (in the transverse direction). Mapping the components by Keulegan-Carpenter number and diffraction parameter classifies each member as small versus large by the dominating physics in that loading regime. The Keulegan-Carpenter number and diffraction parameter are calculated for each of the four components - pontoon, main column, upper column, and base column - over the range of sea states simulated here. The regions where each semi-submersible component fall are illustrated in Fig. 3, where the sea state increases upward and toward the left. The figure demonstrates that the base columns and the upper columns, which comprise the offset columns, fall mostly in the diffraction-dominated region for the sea states considered here. The pontoons fall almost entirely in the inertia and drag

TABLE 2. Current Conditions. The current velocities for the three cases are given at model and prototype-scale. The Reynolds numbers for the four major components of the semi-submersible are presented at model and prototype scale

	Case 1	Case 2	Case 3
Model-Scale Vel.	0.042 (m/s)	0.084 (m/s)	0.14 (m/s)
Model-Scale Re.			
Pontoons	1,356	2,713	4,524
Main Column	5,512	11,024	18,382
Upper Columns	10,176	20,352	33,936
Base Columns	20,352	40,704	67,872
Prototype-Scale Vel.	0.3 (m/s)	0.6 (m/s)	1.0 (m/s)
Prototype-Scale Re.			
Pontoons	480,000	960,000	1,600,000
Main Column	1,950,000	3,900,000	6,500,000
Upper Columns	3,600,000	7,200,000	12,000,000
Base Columns	7,200,000	14,400,000	24,000,000

TABLE 3. Simulated regular wave conditions at prototype scale

Simulated Case	T (s)	H (m)
Regular 1	7.5	1.95
Regular 2	7.7	2.35
Regular 3	8.8	2.75

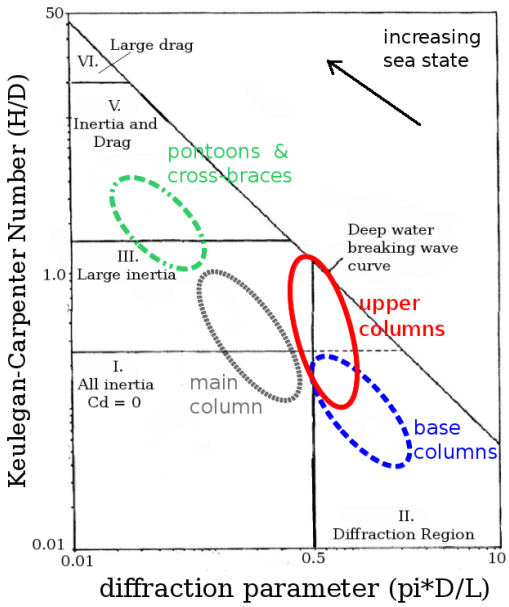

FIGURE 3. Classification of small versus large structures and their limits of applicability. The vertical axis shows H/D, which is equivalent to the Keulegan-Carpenter number, and the horizontal axis is the diffraction parameter. The four major components of the semi-submersible are mapped onto the figure over a range of sea states from 3 to 5, which encompass the range of environmental conditions studied in this paper. Adapted from Chakrabarti [7]. H is the wave height, L is the wave length and D is the characteristic structure diameter

dominated region. The main column spans both sides of the divide between inertia-, drag- and diffraction-dominated regimes.

The classification of structures in Fig. 3 demonstrates the relationship between structure size and dominating physics. The figure is divided by a vertical line that separates the inertia- and drag-dominated regime where Morison's equation is valid, from the diffraction-dominated regime where a panel method code is more appropriate. First, the figure shows that the base and upper columns should be considered as large components, because they are largely dominated by diffraction effects. This is consistent with the decision to include those members in the large components only mesh discussed previously. In addition, the pontoons/cross braces fall in the inertia- and drag-dominated region, which justifies including those members in the small components only mesh. The potential-flow approach is valid everywhere except where viscous effects are important. For this reason, the main column can be modeled with potential-flow theory or Morison's equation, and was classified as a small component in this work. This selection of small and large components is not unique. Second, Fig. 3 illustrates that the simulated wave properties divide the individual components into different dominant load regimes. This allows us to study the assumptions made in HydroDyn where model equations are based on the size of individual components.

3 METHODS

3.1 FAST

FAST is a nonlinear aero-hydro-servo-elastic CAE tool used for wind turbine design. The new FAST (version 8) modularization framework, which is used in the research presented in this paper, breaks the code into several modules including HydroDyn for hydrodynamics. HydroDyn uses a WAMIT potential-flow panel method model as a preprocessor and internal frequency-to-time-domain transforms for time-domain-based potential-flow solutions, as well as an internal Morison's equation solver for

drag effects [5]. In addition, the new release of HydroDyn adds the capability to calculate Morison's equation for multiple interconnected and (nonvertical) platform members.

The WAMIT model developed for this platform is a high-resolution surface model that includes all platform members. This model is used to solve the radiation problem, which generates a body-oscillation frequency-dependent set of coefficients, and the diffraction problem, which generates a vector of wave-frequency dependent coefficients. In this research, the platform is fixed, so there are no forces from radiation, which is caused by platform motion. Furthermore, in current-only cases, there are no waves, so the total force contribution from potential-flow theory is zero.

Morison's equation in its full form includes a term for diffraction-induced wave excitation forces (with a long wavelength approximation), radiation-induced added mass, and viscous drag forces. Only the viscous drag force term of Morison's equation is calculated in this research because the other forces are computed using the potential-flow model. Using the new capabilities of FAST 8, a viscous drag coefficient is specified for every member of the platform. FAST outputs a viscous force prediction per unit length for several nodes along each member. The resulting viscous forces are integrated along the length of each member and summed to produce a resulting total force from Morison's equation. The Morison solution treats each member as an isolated component, neglecting the effects of direct interaction between members. This is not the case for WAMIT, where the diffraction solution includes the effects of direct interactions between members.

3.2 OpenFOAM

This section describes the finite-volume fluid mechanics solver implemented in the open-source CFD software package OpenFOAM described by Weller, et al [8].

3.2.1 Governing Equations The incompressible Navier-Stokes equations, derived from the first principles of conservation of mass and momentum, are solved in the finite-volume framework where the continuous partial differential equations have been recast into a system of linear algebraic equations. The Navier-Stokes equations are employed with a Newtonian relationship between stress and strain.

The VOF approach models multiphase flows, where the fluid phase is identified with a dimensionless scalar function α. The indicator function, α, represents the volume fraction, where a zero value represents fluid "a," and a value of one represents fluid "b." The fluid volume fraction is advected with the flow via a transport equation. The transport equation is solved simultaneously with the mass and momentum conservation equations. Information from cells with a mixed volume-fraction is used to reconstruct the interface between phases.

Initial development of the method can be attributed to Woodward and Noh [9], Hirt and Nichols [10], and deBar [11].

The indicator function, α, is given by [12],

$$\alpha = \begin{cases} 0 & \text{for a point inside fluid "a"} \\ 0 < \alpha < 1 & \text{for a point inside transitional region} \\ 1 & \text{for a point inside fluid "b".} \end{cases}$$

The indicator function, which is chosen to be the volume fraction, is advected with the flow, obeying a transport equation of the form,

$$\frac{\partial \alpha}{\partial t} + (\mathbf{U} \cdot \nabla)\alpha = 0. \tag{1}$$

Because of numerical diffusion, issues arise with convecting a step function such as the volume fraction. To combat these issues, compression of the interface can be achieved via an artificial compression term. This term, first proposed by Weller [12], is shown in the third term in Equation (2).

$$\frac{\partial \alpha}{\partial t} + \nabla \cdot (\mathbf{U}\alpha) + \nabla \cdot (\mathbf{U_r}\alpha(1-\alpha)) = 0. \tag{2}$$

3.2.2 The Numerical Domain and Boundary Conditions As mentioned previously, three meshes are generated representing the full geometry, small components only, and large components only. Each mesh consists of roughly 3 million cells, with increased mesh refinement located around the SWL and near the surface of the semi-submersible body. The model-scale domain begins roughly 9.4 m from the body, extends 4 m past the body in the wave propagation direction, and is 6.3 m wide. The domain depth is 4 m, which matches the depth of the DeepCwind tank tests, and classifies the waves in the deepwater region. At prototype scale, this is equivalent to a mesh that begins 470 m from the body, extending 200 m behind the body, with a depth of 200 m, and a domain width of 315 m. The bottom and sides of the domain are treated as no-slip boundaries. The inlet is treated with varying velocity, volume fraction, and pressure gradient, according to the wave theory being simulated.

A wave library developed for OpenFOAM by Jacobsen, et al, is used in this work [13]. The wave library contains a variety of wave theories, including first-, second-, and fifth-order Stokes waves, as well as cnoidal, solitary, and bichromatic waves. In addition, irregular waves can be generated from the Pierson-Moskowitz and JONSWAP spectra. In this study, only Stokes first order wave theory and steady currents are used.

The time-varying velocity, volume fraction, and pressure gradient are prescribed on the inlet boundary throughout the simulation. Initial conditions can be prescribed as the user wishes.

The simulations presented here have an initially quiescent flow field (i.e. zero velocity everywhere in the domain).

When modeling waves in a numerical domain, it is important to avoid the spurious reflections off numerical boundaries. Jacobsen's wave generation toolbox [13] includes the ability to specify relaxation zones as a method to mitigate artificial wave reflection in the computation domain. Explicit relaxation of the velocity and volume function is implemented to lessen the non-physical reflection of waves off boundaries such as outlets. Relaxation is accomplished via a weighting function that is placed in user specified relaxation zones [13]. This work implements relaxation zones at the domain outlet.

Turbulence is modeled with the Spalart-Allmaras one-equation model [14], with a Spalding wall function at the semi-submersible boundary [15].

3.2.3 Forces and Moments Calculation The load on the body is predicted by integrating the pressure and viscous stresses along the body in a discretized manner. The pressure and viscous forces from each cell face on the surface of the body are summed to find the total pressure and viscous force, respectively. The pressure and viscous forces are then combined to yield a total force on the body. The total moment on the body is calculated as the sum of the moments resulting from pressure and viscous stresses, where moment arms are calculated as the distance from face centers to the structure center of gravity. The total moment is determined in the same manner as the total force. The results are stored as three component vectors, in the x, y, and z directions and in the roll, pitch, and yaw directions for the forces and moments, respectively.

3.2.4 Establishing Confidence in the Computational Fluid Dynamics Models Experimental tests of the model-scale semi-submersible were carried out at the Maritime Research Institute Netherlands (MARIN) under the DeepCwind project, but only for the case of the freely moving body [16]. The simulations carried out in this work model the structure as fixed in place, therefore we cannot directly compare these numerical results to the tank test data. In the absence of experimental data to validate the semi-submersible work against directly, comparable experiments to the case of a fixed semi-submersible in waves and current are used in their place. The CFD model has been validated against a suite of experimental work published in the literature. Uniform flow past a vertical, stationary cylinder is simulated and the drag coefficients across a range of Reynolds numbers are compared to experimental work [17–19]. The case of uniform flow past a stationary cylinder is comparable to the current cases studied in this work. The results from these CFD simulations in OpenFOAM are shown in Fig. 4 alongside various experimental results. The results from this work agree with the experimental results in the literature, establishing confidence in

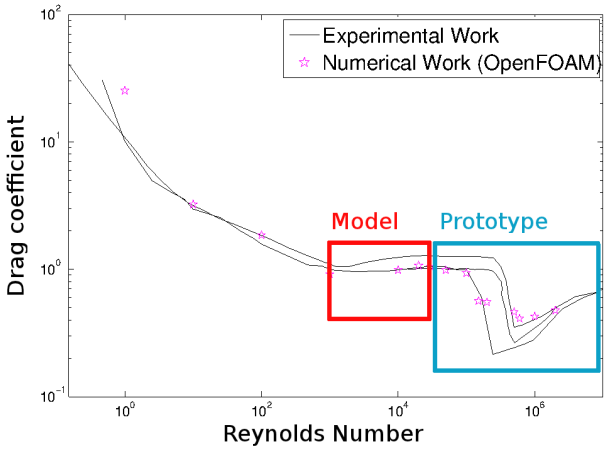

FIGURE 4. Drag coefficient versus Reynolds number for a stationary, vertical cylinder in uniform flow. Experimental results from [17–19] are shown in black lines and these CFD results are shown in pink stars. Model and prototype Reynolds numbers are shown for the semi-submersible in the three current velocities.

the ability of the method described here The ranges of Reynolds numbers for the semi-submersible in the three current velocities simulated in this study are indicated in the figure as well, at the model and prototype scales. The CFD work in this paper is simulated at model scale, where the experimental and numerical results are in excellent agreement.

In addition to validating uniform flow past a stationary body, load predictions in propagating waves are validated in this work. Niedzwecki carried out experiments with a cylinder of radius 0.057 m in a tank with a depth of 0.91 m [20]. Regular waves with a variety of wave properties were generated at the inlet. The experimental work presents the maximum force in the inline direction as a function of the scatter parameter (the wave number times the structure radius).

Wave heights and periods in OpenFOAM were varied to match the wave properties used experimentally. Two meshes were generated and used in simulations, with 1.8 and 2.3 million cells each, including boundary layer refinement on the surface of the cylinder. The time step was controlled by setting the maximum Courant number to 0.5. The gradient term was discretized with a first-order Gauss scheme, and a total variation diminishing (TVD) scheme was used to discretize the convection term to achieve accuracy and boundedness. Figure 5 shows the numerical versus experimental results for the maximum force in the inline (wave propagation) direction. It can be seen that for a range of scatter parameters, the predicted maximum inline force predicted by OpenFOAM is in good agreement with the experimental measurements presented by Niedzwecki [20].

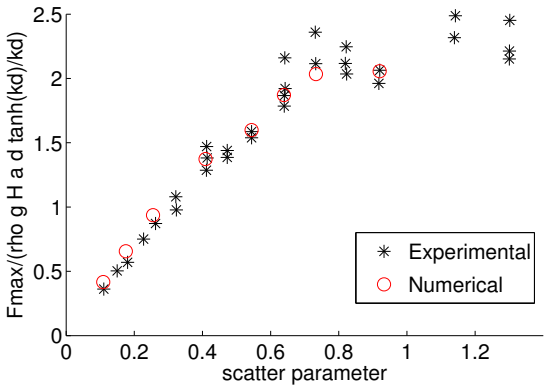

FIGURE 5. Inline force on a stationary, vertical cylinder in propagating regular waves versus the scatter parameter. Experimental results by Niedzwecki [20] shown in black asterisks, our CFD results are represented with red circles. *rho* is density, *g* is gravity, *a* is the cylinder radius, *d* is water depth, *H* is the wave height and *k* is the wave number.

4 RESULTS AND DISCUSSION

Following the validation exercises, simulations of the semi-submersible in current and regular waves are carried out in both OpenFOAM and FAST in each of the environmental conditions described in Section 2.2. OpenFOAM simulations are conducted with each of the three representative geometry meshes at model scale. FAST simulations are performed at prototype scale. All results from OpenFOAM have been scaled to prototype scale using Froude scaling.

The current cases are dominated by drag effects, which are calculated with Morison's equation. The loading on the structure in regular waves is dominated by diffraction, and the contributions from Morison's equation are negligible. First, the results for the semi-submersible in current are presented, followed by results for the structure in regular waves.

4.1 Current Results

Inline and transverse force predictions are presented for the semi-submersible in a current with velocity of 0.6 m/s in Fig. 6. OpenFOAM results are presented from simulations with the three representative geometry meshes described earlier. Results from the large component only mesh, small component only mesh and the full geometry mesh are shown by the solid blue line, dashed red line, and light blue line, respectively. Force predictions from FAST are represented by the dash-dotted black line.

The inline force prediction from FAST is larger than any of the inline force results from OpenFOAM. One possible reason for these differences is due to the numerical treatment of shadowing effects. The simulations in OpenFOAM naturally account for shadowing effects, in which downstream members are shadowed by upstream members, decreasing the load. These shadowing effects are not accounted for in FAST, and each member is assumed to interact with an undisturbed flow. Future work will examine the shadowing effect in more detail. The discrepancy may also be due to the fact that OpenFOAM predicts drag co-

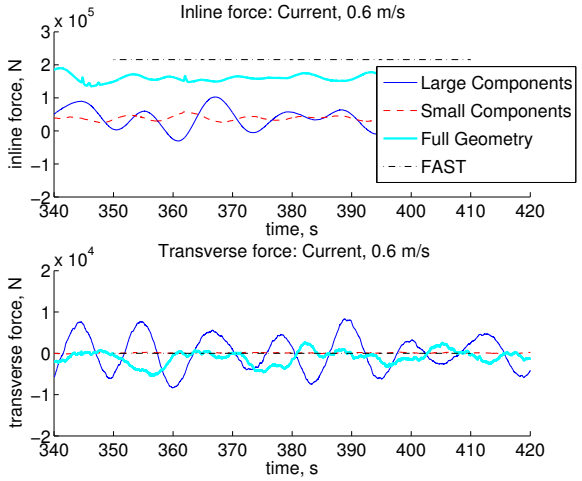

FIGURE 6. Inline and transverse force results from OpenFOAM and FAST. Results from the large components only, small components only and full geometry meshes are shown for OpenFOAM. FAST predicts a larger inline force, but smaller transverse force compared to OpenFOAM.

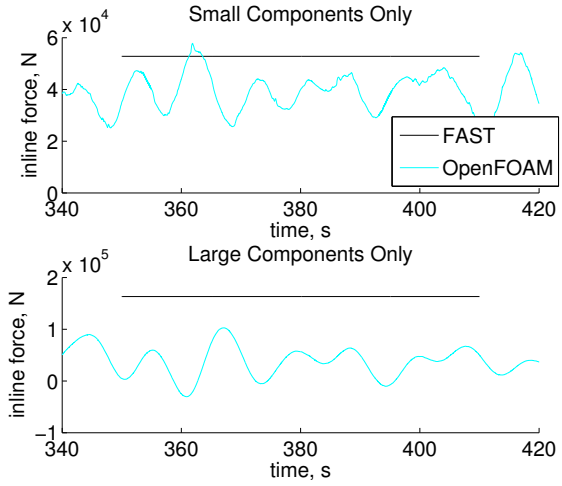

FIGURE 7. Inline force predictions from FAST and OpenFOAM for only the small components, and only the large components in a current of 0.6 m/s. FAST predicts a larger force on both small and large components.

efficients that are between 2.0% and 8.4% lower than the value of 1.0 used in FAST. It may also be the case that a drag coefficient of 1.0 in FAST is not appropriate for all members. FAST predicts a constant zero force in the transverse direction, which is not representative of the true time-varying physics that result from vortex shedding, just as it is expected from the Morison formulation. The results from OpenFOAM properly capture the time-varying nature of the transverse force, unlike the FAST results that do not model the vortex shedding and associated lift forces.

In addition to looking at the total hydrodynamic loading on the semi-submersible, forces on individual components are examined. The total forces on the small components, which include the pontoons, cross braces, and main column, are summed from the FAST output and compared to the results from the OpenFOAM simulation with the small components only mesh. Additionally, the sum of the forces on the large components in FAST are compared to the results from the large components only mesh in OpenFOAM. The comparison of inline forces in a current of 0.6 m/s is shown in Fig. 7. For both the small and large components, FAST predicts larger inline forces, where the difference is greater for the case of large components. This is consistent with the expectation that Morison's equation predicts forces more accurately for small components. Again, the larger predicted forces from FAST may be the result of neglecting shadowing effects of upstream members sheltering downstream members, or also the difference in drag coefficients between FAST and OpenFOAM.

Figure 8 summarizes the overall effect of the velocity on the force predictions from the three steady current cases by comparing the mean of the forces in the inline and transverse directions. In current, FAST predicts constant forces in the inline and transverse directions. OpenFOAM predicts oscillating forces, which more closely match the physics. Error bars on the OpenFOAM results indicate the standard deviation from the mean because of the time-varying nature of these signals. Only the full geometry results from OpenFOAM are considered here. Again, FAST predicts a larger inline force than OpenFOAM, which could be a consequence of shadowing effects being neglected in FAST.

FAST predicts a zero transverse force across all current velocities. OpenFOAM shows a slight nonzero mean that results from noise in the transverse force signal. The standard deviation in the transverse force prediction from OpenFOAM (shown by the error bars in Fig. 8) demonstrates that the two codes are in fair agreement for the mean transverse flow predictions. Transverse force prediction in OpenFOAM does capture lift forces, which are not computed in FAST because it uses Morison's equation.

The full geometry load prediction from OpenFOAM does not equal the sum of the results from the large components only and the small components only meshes. This is likely due to the complex flow patterns that result from the fluid interacting with the structural components in the interior region of the semi-submersible. The accelerating flow around and through the full

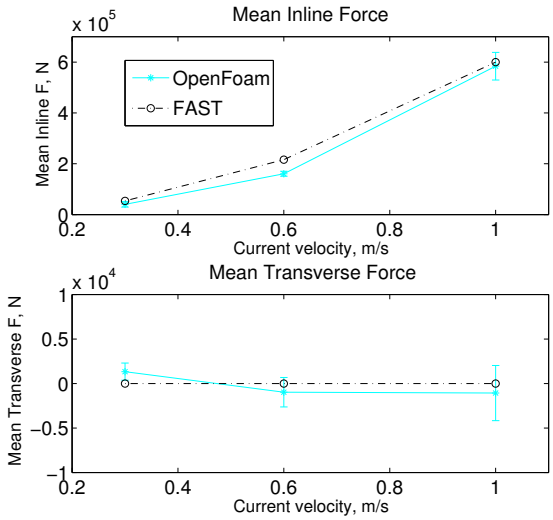

FIGURE 8. Trends in the inline and transverse force predictions in steady current. The mean of the inline and transverse forces from both codes is plotted against increasing current velocities. Error bars on the OpenFOAM results illustrate the standard deviation from the mean because the inline and transverse forces are actually oscillating signals. FAST predicts a larger inline force at all three current velocities. FAST predicts a zero transverse force across all currents; while OpenFOAM has a slightly nonzero mean transverse force because of noise, with standard deviations that encompass the prediction from FAST.

geometry mesh results in an increased load prediction on the structure.

4.2 Regular Wave Results

The current-only cases provide insight about the Morison's equation component of FAST. The regular wave cases shed light on the potential-flow theory portion of FAST. Load contributions from Morison's equation are negligible compared to diffraction forces for the regular wave cases investigated in this work. FAST calculates the diffraction forces from coefficients produced in WAMIT. Contributions from Morison's equation and diffraction are compared in Fig. 9. Radiation forces are omitted from the figure because they are zero for this case of the nonmoving structure.

OpenFOAM and FAST results from the Regular 2 wave case, with properties given in Table 3, are shown in Fig. 10. The inline-force results from FAST and the full geometry case in OpenFOAM show excellent agreement. Previously with the steady current simulations there was sizable disagreement between the inline force predictions, but now the load contributions from drag are negligible compared to contributions from diffraction. The semi-submersible is now in a regime where diffraction

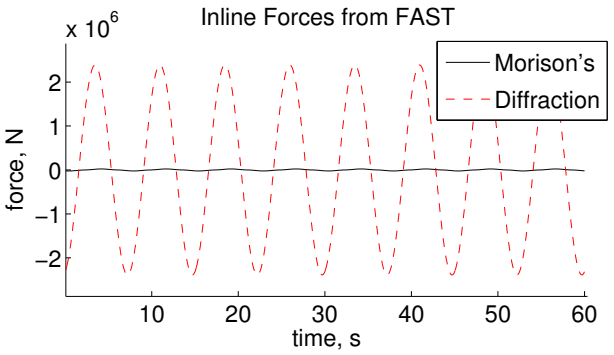

FIGURE 9. Inline forces from FAST. The solid black line shoes the forces resulting from Morison's equation, and the red dotted line represents loading from diffraction, calculated in HydroDyn. The plot illustrates that drag forces calculated with Morison's equation are negligible compared to diffraction for the semi-submersible in Regular 2 waves.

effects are dominant, unlike in the current cases. The diffraction forces from WAMIT include the interaction between members such that shadowing should play a lesser role. Again, the differing drag coefficients in FAST and OpenFOAM may be the cause for discrepancy in force predictions. As was the case for current, FAST predicts a constant zero transverse force; OpenFOAM gives a time varying transverse force. The heave forces are also presented, where FAST predicts a slightly larger force compared to OpenFOAM for all representative geometries. As expected, the large components only and small components only meshes predict smaller heave forces, which is a direct result of their smaller volume and surface area.

Results from the two codes are compared across the range of wave heights simulated in this study, and are illustrated in Fig. 11. The means of the inline, transverse, and heave forces from both FAST and OpenFOAM's full geometry mesh are shown in the plots from top to bottom, respectively. The error bars indicate the standard deviation from the mean force. The inline force predictions from FAST and OpenFOAM are in excellent agreement across the range of wave heights. The transverse force predicted by OpenFOAM grows with increasing wave height, yet remains zero in the FAST output. The heave force prediction is larger in FAST than OpenFOAM, across all wave heights studied here. Unlike with the current cases, where the absence of shadowing effects in FAST may be the source of large discrepancies in inline force results between the two codes, the inline force predictions from the two codes agree well for the semi-submersible in waves. Again, the lack of a lift force in FAST causes disagreement between the two codes, just as it did for the current cases. The discrepancy in lift force predictions is more important for the current-only cases, and less important for wave cases where drag and lift forces are negligible compared to diffraction loads. Even though the OpenFOAM results demonstrate that the transverse force is of smaller magnitude than the inline force, the loading in the transverse direction should not be ignored.

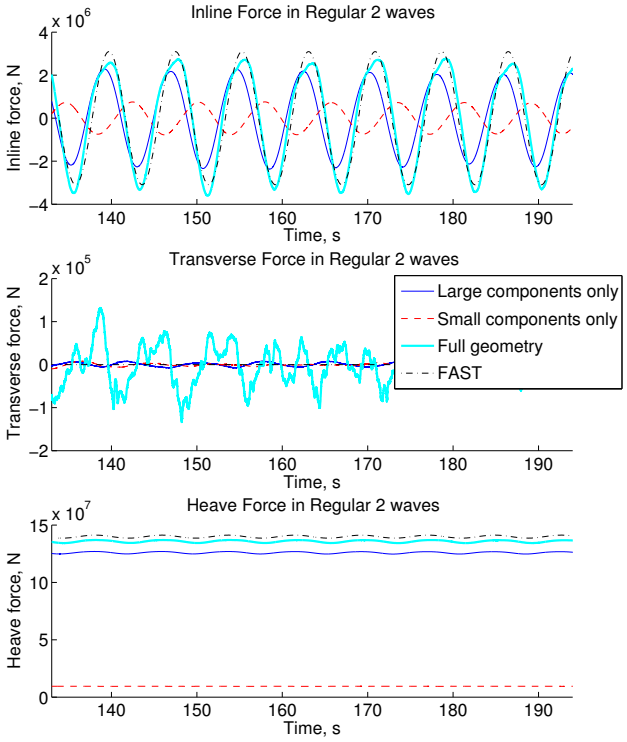

FIGURE 10. Inline, transverse and heave force results from OpenFOAM and FAST. Results from the large components only, small components only and full geometry meshes are shown for OpenFOAM. FAST and OpenFOAM show excellent agreement for the inline force, while the transverse flow prediction is much greater from OpenFOAM than it is from FAST. The heave force prediction is larger in FAST than it is in OpenFOAM.

5 CONCLUSIONS

A code-to-code comparison was carried out between the HydroDyn module in FAST, a CAE tool for assessing hydrodynamics loads on offshore wind turbines, and OpenFOAM, a high-fidelity CFD software package. A fixed semi-submersible was simulated in current-only and waves-only conditions to assess differences in load predictions in the two codes. Confidence in the ability to accurately model rigid bodies in current and wave conditions with OpenFOAM, based on previous validation exercises, is high.

First, a series of current-only cases were simulated in FAST

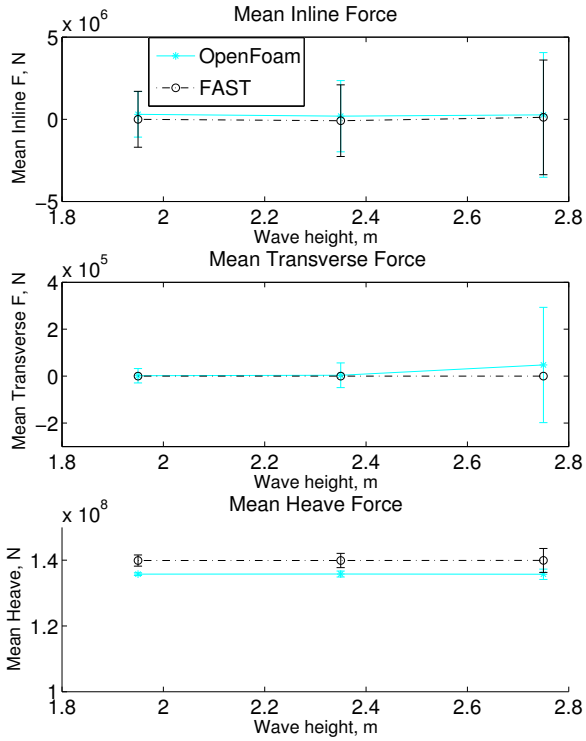

FIGURE 11. Trends in the mean inline, transverse, and heave force predictions in regular waves. The mean values of the inline force predictions with increasing wave height are demonstrated in the top plot. The mean transverse and heave forces are given in the middle and bottom plots, respectively. Standard deviation from the mean in OpenFOAM is illustrated with error bars. Excellent agreement was found between FAST and OpenFOAM inline loading predictions. The transverse force prediction from FAST is zero for all wave heights, and increases with increasing wave height in OpenFOAM. The mean heave force prediction is larger from FAST for across all wave heights studied here.

and OpenFOAM. Comparison of load predictions from the two codes showed larger drag forces from FAST than from OpenFOAM. This may be the result of the natural simulation of shadowing effects in OpenFOAM, where downstream members are shielded by upstream members, or from differences in the drag coefficient. HydroDyn uses Morison's equation, which does not account for lift forces that occur because of vortex shedding, unlike OpenFOAM, which captures the time-varying force in the transverse flow direction.

Next, wave-only conditions were simulated for a range of wave heights and periods. In these cases, the inline-force predictions from FAST and OpenFOAM were in excellent agreement, but again, the FAST results did not capture any lift forces. The magnitude of the transverse force is smaller than the inline force, but it is still significant.

The ability to capture shadowing effects and transverse forces from vortex shedding would enhance HydroDyn's load predictions, and other engineering codes that employ similar assumptions and theories. Future work will examine the role of shadowing in load predictions from each code, as well as further investigate the drag coefficients in each code.

Future work will simulate the semi-submersible with free 6-DOF body motion in FAST and OpenFOAM. Results will be compared to experimental results from the DeepCwind project carried out at MARIN to validate the improvements made in FAST 8 and provide further insights into the physics by investigating high-fidelity results from OpenFOAM. OpenFOAM will also supplement the experimental data set by simulating extreme conditions not simulated in the wave tank.

ACKNOWLEDGMENT

The authors would like to acknowledge the support of a grant from the Department of Energy, award number DE-AC36-08GO28308. This work used the Extreme Science and Engineering Discovery Environment (XSEDE), which is supported by National Science Foundation grant number OCI-1053575. The authors acknowledge the Texas Advanced Computing Center (TACC) at The University of Texas at Austin for providing high performance computing resources that have contributed to the research results reported within this paper. http://www.tacc.utexas.edu for more information.

REFERENCES

[1] Musial, W., and Ram, B., 2010, "Large-scale Offshore Wind Power in the United States: Assessment of Opportunities and Barriers," NREL/TP-500-40745, National Renewable Energy Laboratory.

[2] Musial, W., 2007, "Offshore Wind Electricity: A Viable Energy Source for the Coastal United States," Mar. Technol. Soc. J., **41**, pp. 32-43.

[3] Jonkman, J., 2009, "Dynamics of Offshore Floating Wind Turbines Model Development and Verification," Wind Energy, 12: pp. 459 -492.

[4] Jonkman, J., and Matha, D., 2011, "Dynamics of Offshore Floating Wind Turbines Analysis of Three Concepts," Wind Energy, **14**(4), pp. 557 - 569.

[5] Jonkman, J., and Buhl, M. L., 2006, "FAST User's Guide," NREL/EL-500-38230, National Renewable Energy Laboratory, Golden, CO.

[6] Robertson, A., Jonkman, J., Masciola, M., Song, H., Goupee, A., Coulling, A., and Luan, C. "Definition of the Semisubmersible Floating System for Phase II of OC4," National Renewable Energy Laboratory, Golden, CO.

[7] Chakrabarti, S. K., 2005, "Handbook of Offshore Engineering," Elsevier, Boston, MA.

[8] Weller, H., Tabor, G., Jasak, H., and Fureby, C., 1998, "A Tensorial Approach to Computational Continuum Mechanics Using Object-oriented Techniques," Comput. Phys., **12** pp.620 - 631.

[9] Noh, P. and Woodward, P., 1976, "SLIC (Simple Line Interface Calculation)," 5th International Conference on Fluid Dynamics, 59.

[10] Nichols, B. D. and Hirt, C. W., 1975, "Methods for Calculating Multi-dimensional Transient Free-surface Flows Past Bodies," Technical Report, Los Alamos National Lab, NM.

[11] DeBar, R., 1947, "Fundamentals of the KRAKEN Code," Technical Report, UCIR-760, Lawrence Livermore National Lab, CA.

[12] Rusche, H., 2002, "Computational Fluid Dynamics of Dispersed Two-Phase Flows at High Phase Fractions," Imperial College of Science, Technology and Medicine, London.

[13] Jacobsen, N. G. and Fuhrman, D. R. and Fredsøe, J., 2011, "A Wave Generation Toolbox for the Open-source CFD Library: OpenFoam," International Journal for Numerical Methods in Fluids.

[14] Spalart, P. R., and Allmaras, S. R., 1992, "A One-Equation Turbulence Model for Aerodynamic Flows," American Institute of Aeronautics and Astronautics (AIAA) Paper 92-0439, AIAA, Reston, VA.

[15] Spalding, D. B., 1961, "A Single Formula for the Law of the Wall," Trans. ASME., J. Appl. Mech. **28**(3) pp. 444-458.

[16] de Ridder, E. J., Koop, A. H., and van Doeveren, A. G., 2001, "DeepCWind Floating Wind Turbine Model Tests," Volume I. Report No. 24602-1-OB, Wageningen, Netherlands.

[17] Sarpkaya, T., and Isaacson, M., 1981, "Mechanics of Wave Forces on Offshore Structures," Van Nostrand Reinhold, New York, NY, pp. 651-652.

[18] Delany, K., and Sorensen, E., 1953, "Low-speed Drag of Cylinders of Various Shapes," Nat. Adv. Comm. Aero., Washington, Technical Note 3038.

[19] Lindsey, W. F., 1923, "Drag of Cylinders of Simple Shapes," Report No. 619.

[20] Niedzwecki, J. M., 1992, "Wave Runup and Forces on a Circular Cylinder in Regular and Random Waves," J. of Waterway, Port, Coastal, Ocean Eng. **6**(118), pp. 615-620